

# Accepted Manuscript

Role of defects on the magnetic behaviour of the geometrically frustrated spinel  
 $\text{ZnFe}_2\text{O}_4$

K.L. Salcedo Rodríguez, S.J. Stewart, P.M. Mendoza Zélis, G.A. Pasquevich, C.E.  
Rodríguez Torres

PII: S0925-8388(18)31474-9

DOI: [10.1016/j.jallcom.2018.04.172](https://doi.org/10.1016/j.jallcom.2018.04.172)

Reference: JALCOM 45810

To appear in: *Journal of Alloys and Compounds*

Received Date: 13 January 2018

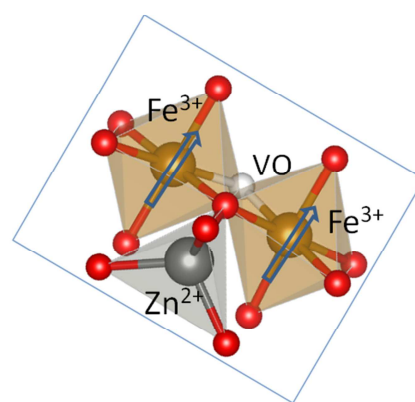
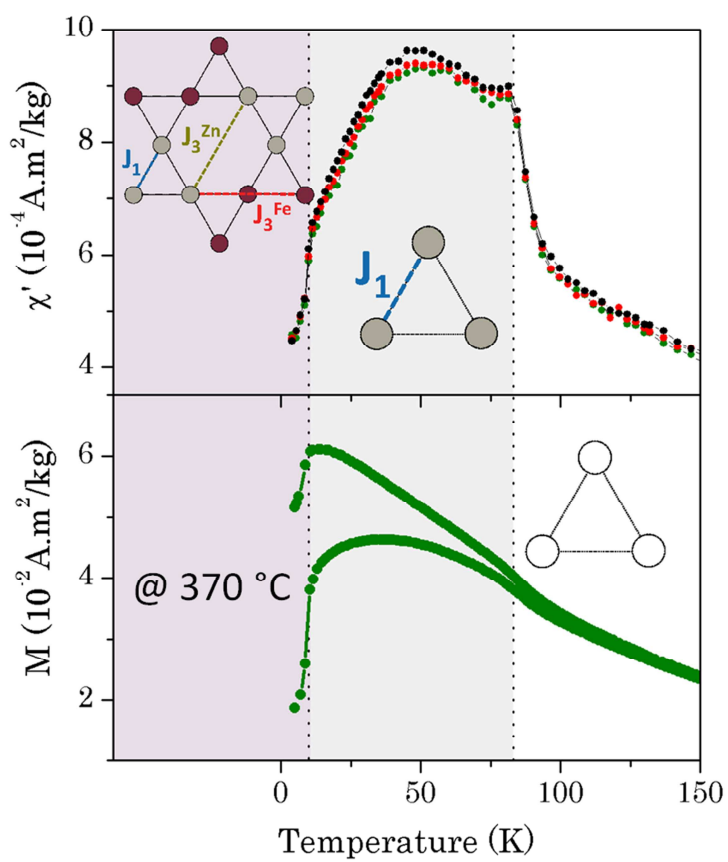
Revised Date: 17 March 2018

Accepted Date: 13 April 2018

Please cite this article as: K.L. Salcedo Rodríguez, S.J. Stewart, P.M. Mendoza Zélis, G.A. Pasquevich, C.E. Rodríguez Torres, Role of defects on the magnetic behaviour of the geometrically frustrated spinel  $\text{ZnFe}_2\text{O}_4$ , *Journal of Alloys and Compounds* (2018), doi: 10.1016/j.jallcom.2018.04.172.

This is a PDF file of an unedited manuscript that has been accepted for publication. As a service to our customers we are providing this early version of the manuscript. The manuscript will undergo copyediting, typesetting, and review of the resulting proof before it is published in its final form. Please note that during the production process errors may be discovered which could affect the content, and all legal disclaimers that apply to the journal pertain.





ACCEPTED

**Role of defects on the magnetic behaviour of the geometrically frustrated spinel****ZnFe<sub>2</sub>O<sub>4</sub>**

K. L. Salcedo Rodríguez, S. J. Stewart<sup>#</sup>, P. M. Mendoza Zélis, G. A. Pasquevich and C. E.

Rodríguez Torres

<sup>1</sup>IFLP-CCT- La Plata-CONICET and Departamento de Física, Facultad de Ciencias

Exactas, C. C. 67, Universidad Nacional de La Plata, 1900 La Plata, Argentina

**Abstract**

Defective zinc ferrites ZnFe<sub>2</sub>O<sub>4-δ</sub> obtained by vacuum annealing bulk Zn-ferrite at different temperatures  $T_{\text{Ann}}$  were investigated by using XANES at Zn-K, Fe-K and XMCD at Fe-L<sub>2,3</sub> edges, static and dynamic magnetic measurements. The cation inversion that confers to the starting ferrite a weak ferromagnetic response is progressively lost when  $T_{\text{Ann}}$  surpasses 250 °C. Consequently, there is a detriment of the magnetic response that reaches its lower value for  $T_{\text{Ann}}$  around 370 °C, being the latter coincident with a negligible non-equilibrium occupancy. Above  $T_{\text{Ann}} \sim 450$  °C the ferrite progressively enhances its magnetic response. In such case, even though Zn and Fe occupy non-equilibrium sites at surface regions, the deficiency of oxygen predominates over inversion and the former triggers an increment of the magnetic coupling between Fe<sup>3+</sup> at octahedral spinel sites. We discuss the magnetic results that account for spin-glass and/or cluster-glass behavior of this geometrically frustrated compound as due to the randomness and frustration introduced by local defects.

*Keywords:* zinc ferrite, ZnFe<sub>2</sub>O<sub>4</sub>, geometrically frustrated spinel, pyrochlore, cluster glass

*<sup>#</sup>Corresponding author:* stewart@fisica.unlp.edu.ar

**1. Introduction**

Zinc ferrite ZnFe<sub>2</sub>O<sub>4</sub> has a spinel structure where in its normal state Zn<sup>2+</sup> and Fe<sup>3+</sup> occupy, respectively, 8 tetrahedral (A) and 16 octahedral [B] interstitial sites of an *fcc* oxygen unit superlattice [1]. In spite that ZnFe<sub>2</sub>O<sub>4</sub> is widely identified as an antiferromagnet with a Néel temperature ( $T_N$ ) around 10 K [2], neutron scattering results have cast doubt on whether

this compound intrinsically displays a long-range order (LRO) or it is driven by the presence of defects [3-5]. While the susceptibility shows a peak near  $T_N$ , its positive Curie-Weiss temperature  $\Theta_{CW} \sim +120$  K (or higher) and the lack of evidence of a LRO at least down to 1.5 K for high-purity single-crystal of  $ZnFe_2O_4$  suggest the existence of a strong spin frustration [4,6]. Actually,  $ZnFe_2O_4$  can be modeled as a Heisenberg 3D-geometrical frustrated system where the B-sites form a network of corner-sharing tetrahedra (pyrochlore-type) from neighboring  $BO_6$  octahedra [3, 4, 7]. Therefore, its unusual magnetic behavior has been interpreted as driven by the third-neighbor antiferromagnetic (AF) interactions  $J_3$  (paths B-O-B-O-B and B-O-A-O-B) that compete with the temperature-dependent first-neighbor ferromagnetic (FM) interactions  $J_1$  (B-O-B) [6,8,9]. While the FM spin correlations dominate at high temperatures, the AF interactions become important below  $\sim 15$  K [9]. At the lowest measured temperatures, the geometrically frustrated system is expected to remain in a disordered state due to the degeneracy of its ground state [5,10].

Within this scenario, the broken symmetry generated by localized defects such as cationic inversion, impurities or vacancies might give rise to a relief of the geometrical frustration and, at the same time, to the emergence of other competing interactions and randomness that lead to novel magnetic properties. One remarkable result concerning the presence of such defects in the  $ZnFe_2O_4$  lattice is the appearance of a spontaneous magnetization at room temperature [11-15]. This property also encourages developments for potential applications of this ferrite as part of chemically stable and low-cost products with semiconducting and magnetic properties [15,16].

The cation inversion in  $\text{ZnFe}_2\text{O}_4$  implies that some  $\text{Fe}^{3+}$  replace  $\text{Zn}^{2+}$  ions at sites (A) and the  $\text{Zn}^{2+}$  go to [B] sites. This modifies the superexchange interactions and, depending on the degree of inversion (i. e., the fraction of  $\text{Fe}^{3+}$  at (A) sites), the ferrite displays a variety of spin arrangements, like ferrimagnetism, cluster or spin-glass-like behaviors [3,17,18]. One way to obtain partially inverted ferrites at ambient temperature consists of performing a quenching from high temperatures [19,20,21]. The state of inversion is mainly a feature distinctive of nanosized  $\text{ZnFe}_2\text{O}_4$ , where the tetrahedral symmetry of  $\text{Fe}^{3+}$  is naturally broken. However, it is still unclear what the relationship between the degree of inversion and the particle size is (see, for instance, [3,11,22]).

The oxygen deficiency can also be a key factor to alter the  $\text{ZnFe}_2\text{O}_4$  intrinsic behavior, because gives rise to interrupted superexchange paths and to the rearrangement of the ions' positions [12,14,17,20,23]. For instance, the enhancement of the magnetic response observed in  $\text{ZnFe}_2\text{O}_4$  nanoparticles annealed under vacuum [12, 23] and thin films growth at low oxygen partial pressure [14-17] has been attributed to the presence of oxygen vacancies (VO). Additionally, the cluster-glass C-G magnetic behavior observed in  $\text{ZnFe}_2\text{O}_{4-\delta}$  films was interpreted as due a random distribution of zinc and iron atoms generated by vacancies [17]. However, the influence of VO on the magnetism of zinc ferrite is difficult to be discriminated in these nanosystems because their magnetic response is usually affected not only by a considerable state of inversion but also by superparamagnetic relaxation and surface effects.

On the other side, density-functional-theory DFT calculations performed on  $\text{ZnFe}_2\text{O}_4$  predict that the VO in  $\text{BO}_6$  octahedron bring about a local ferromagnetic FM coupling between iron ions at [B] sites affecting its magnetic ordering [14]. More recently,

additional first-principles calculations performed by Yao *et al.* [24] showed that the VO in  $\text{ZnFe}_2\text{O}_4$  induce a distortion of the unit cell structure and significantly weaken the strength of Zn-O bonds and increase the Fe-O ones around VO. Consequently, this causes an alteration of superexchange integrals that affects the intensity of the competing interactions.

All the experimental and theoretical findings point toward that the presence of vacancies in  $\text{ZnFe}_2\text{O}_4$  strongly impacts on its magnetic behavior, hence their effects worthwhile to be explored more in deep. Considering that most of the studies have been performed in nanosized  $\text{ZnFe}_2\text{O}_4$  whose behavior is affected by size effects and an unavoidable state of partial inversion, more studies on bulk material are needed to further understand the influence of VO on the magnetic behavior of this geometrically frustrated ferrite. To this end, we present here an investigation on zinc ferrite bulk powders that were subjected to vacuum annealing at different temperatures up to 620 °C. We describe the structural, electronic and magnetic behavior of these defective ferrites using x-ray diffraction, near edge x-ray absorption spectroscopy (XANES), magnetic circular dichroism (XMCD), static and dynamic magnetic measurements.

## 2. Experimental

Polycrystalline ferrite  $\text{ZnFe}_2\text{O}_4$  was obtained by conventional solid state reaction from a  $\alpha$ - $\text{Fe}_2\text{O}_3$  and ZnO stoichiometric mixture annealed in air at 1000 °C during 24 hours. The annealing was repeated with intermediate grinding. The as-prepared single phase ferrite (ZFO) was divided into several batches that were thermally treated under a vacuum pressure ( $p_0=1.5 \times 10^{-4}$  Torr). These treatments were performed using a tubular furnace with a temperature gradient. This set-up allows annealing several batches simultaneously at

different temperatures and keeping the same  $p_O$ . Two sample series were prepared from ZFO: Series I (furnace range temperature from 25 to 450°C) and Series II (from 240 to 620°C). The as-annealed samples of both series were labeled as ZFO- $T_{Ann}$ , where  $T_{Ann}$  stands for the annealing temperature sensed at the middle point of a sample position.

X ray diffraction (XRD) patterns of samples of Series I were recorded with a X'Pert diffractometer (CuK $\alpha$ ,  $\lambda=1.5406$  Å). The data were collected in the  $20^\circ \leq 2\theta \leq 80^\circ$  range scanned with an angle step of  $0.02^\circ$ . Diffractograms of Series II were collected at the XRD beam line of the Brazilian Synchrotron (LNLS). The data were collected with a monochromatic X-ray beam,  $\lambda = 1.24106$  Å in the  $8^\circ \leq 2\theta \leq 90^\circ$  range scanned with an angle step of  $0.005^\circ$ . All these data were indexed and refined using the MAUD program [25].

X ray absorption near edge spectra (XANES) were collected in transmission mode room temperature at the D04B-XAFS1 beam line of LNLS around the Fe and Zn K-edges (7112 and 9662 eV, respectively). XMCD experiments at the  $L_{2,3}$  edges were performed at room temperature in the PGM beamline at LNLS by using the circularly polarized light with the degree of circular polarization around 80%. The absorption data were collected in the total electron yield (TEY) mode. The photon beam was perpendicular to the sample and a magnetic field  $\mu_0 H_{ap} = 1$ T was applied normal to the sample plane. The absorption has been normalized to the incoming photon beam intensity by measuring synchronously the photocurrent at a gold grid. The absorption cross section of the circular polarized x-rays is labeled  $\mu^{\alpha\beta}$ , where  $\alpha$  denotes the helicity of the photon ( $\alpha=\uparrow$  ( $\downarrow$ ) when the photon are right-hand (left-hand) polarized) and  $\beta$  denotes the direction of  $H_{ap}$  ( $\beta=\uparrow$  ( $\downarrow$ ) when the field is parallel (antiparallel) to the propagation vector). In the electric dipole approximation

reversing  $H_{ap}$  is equivalent to changing beam helicity, thus  $\mu^{\uparrow\uparrow} = \mu^{\downarrow\downarrow}$  and  $\mu^{\uparrow\downarrow} = \mu^{\downarrow\uparrow}$ . The XMCD signal was obtained from  $\mu_{XMCD} = (\mu^{\uparrow\uparrow} + \mu^{\downarrow\downarrow} - \mu^{\uparrow\downarrow} - \mu^{\downarrow\uparrow})/2$ , and normalized by the area of the corresponding XANES spectrum.

Magnetization ( $M$ ) as a function of applied magnetic field ( $H$ ) was obtained using vibrating sample magnetometer (VSM) from LakeShore and a superconducting quantum interference device (SQUID) from Quantum Design. The later was also employed to measure the  $M$  vs.  $H$  loops at 5 K and the thermal dependence of  $M$  under zero field cooling (ZFC) and field-cooled (FC) conditions with a cooling field  $H_{FC} = 8$  kA/m. The in-phase  $\chi'$  and out-of-phase  $\chi''$  components of the AC susceptibility were recorded between 20 and 325 K in a LakeShore 7130 susceptometer using field amplitude of 0.08 kA/m and frequencies in the 50 Hz to 10 kHz range. Additional AC susceptibility measurements in the 2 to 120 K temperature range for samples ZFO-250, ZFO-370 and ZFO-580 were performed using the SQUID magnetometer.

### 3. Results

The XRD patterns (see Supporting Information S.I.) showed that all samples are single phase of the *fcc* spinel structure (SG  $Fd-3m$ ). The lattice parameter  $a$  estimated for sample ZFO is  $8.44 \pm 0.01$  Å, in good agreement with the ICDD data of  $ZnFe_2O_4$  (PDF #821042). Within uncertainties, none of the  $a$  values obtained for Series I and II showed appreciable changes with respect to the cell parameter of ZFO. It is worth mentioning that the color of the samples changes from light to dark brown as  $T_{Ann}$  increases (see S.I.).

Figures 1 and 2 exhibit, respectively, the Zn and Fe K-edge XANES spectra of selected samples ZFO, ZFO-370 and ZFO-620. In all cases, the Zn K-edge spectra present the



typical shape of  $\text{ZnFe}_2\text{O}_4$  XANES that accounts for electronic transitions from  $1s$  to unoccupied  $p$  states, i. e., three resolved peaks A, B and C as well as a shoulder D (Fig. 1(a)) [11]. Even though the spectra are all similar, we observe that the peaks' intensities vary with  $T_{\text{Ann}}$ . Indeed, the B to A peak intensity ratio ( $I_{\text{B}}/I_{\text{A}}$ ) first decreases with  $T_{\text{Ann}}$  up to  $400\text{ }^\circ\text{C}$ , then starts to increase for higher  $T_{\text{Ann}}$  (Fig. 1 (b)). On the other hand, the intensity of peak D reaches a maximum for ZFO-370 (Fig. 1 (c)). The initial trends, i. e., the  $I_{\text{B}}/I_{\text{A}}$  decrease as well as the increase of  $I_{\text{D}}$  are compatible with a progressive disappearance of a slight degree of inversion present in the starting sample (see discussion below) [11].

The Fe K-edge XANES results (Fig. 2(a)) also point toward a progressive approach of ZFO to an ideally normal ferrite for  $T_{\text{Ann}}$  up to ca.  $370\text{ }^\circ\text{C}$  because less Fe ions occupy (A) sites [11, 26]. Indeed, this is reflected by the increment of the pre-edge peak intensity ( $1s \rightarrow 3d$  and  $1s \rightarrow 3d/4p$  electronic transitions) (Fig. 2 (b)) and the decrease of the white line ( $1s \rightarrow 4p$ ) (Fig. 2 (c)) [11, 26,27]. The opposite trend of the ZFO-620 spectrum indicates that a reoccupation of (A) sites by iron ions has taken place [11,26,27] producing an increment of the degree of orbital  $p$ - $d$  mixing. On the other hand, all spectra show similar edge energies corresponding to Fe ions with +3 oxidation state [27]. The possible presence of  $\text{Fe}^{+2}$  ions is below the detection limit.

The Fe L-edge XMCD spectra (Fig. 3) allow us to distinguish between the contributions of iron ions sitting either at tetrahedral ( $\text{Fe}_{\text{A}}$ ) or octahedral ( $\text{Fe}_{\text{B}}$ ) sites [14]. The two negative peaks (B1 and B2 in Fig. 3) correspond to  $\text{Fe}_{\text{B}}$  aligned parallel to  $H_{\text{ap}}$  while positive signal (peak A1) correspond to  $\text{Fe}_{\text{A}}$  that align antiparallel to  $H_{\text{ap}}$ . The fact that the XMCD signal of ZFO presents a no null contribution from  $\text{Fe}_{\text{A}}$  confirms that this sample presents some

inversion. It is worth mentioning that the TEY mode used to perform the XMCD measurements is surface sensitive (about 5 nm in depth), thus the detected site inversion involves those iron ions at grain surfaces. After annealing at 370 °C, the A1 peak almost disappears while B1 and B2 contributions also decrease, in accordance with the reduction of the degree of inversion [14]. On the other side, we observe that increasing  $T_{\text{Ann}}$  above 370 °C the  $\text{Fe}_B$  contribution increases.

$M$  vs.  $H$  loops were registered at 5 and 300 K (Fig. 4). For all samples, the response consists of a superposition of two contributions: i) a paramagnetic (PM) component that accounts for the linear behavior of  $M$  at high-fields and ii) a ferromagnetic-like component that gives rise to the S-shape at low-fields. The room temperature magnetic response at high fields ( $\mu_0 H > 0.7$  T) were fitted using the following equation:

$$M(H) = \chi_p H + M_s (1 - a/|H| - b/H^2) \quad (1)$$

where  $\chi_p$  is the high-field PM susceptibility and  $M_s$  is the saturation magnetization [28]. The tendency of the resulting parameters  $\chi_p$  and  $M_s$  clearly shows that for  $T_{\text{Ann}}$  above 370 °C, there is an increment of the magnetic response (Figs.4(c) and 4(d)).

At  $T=5$  K, while the  $M$  vs.  $H$  loop of ZFO-as-cast shows hysteresis with a coercive field  $\mu_0 H_C \sim 28$  mT, the hysteresis almost disappears when  $T_{\text{Ann}}$  is above 370 °C. On the contrary, loops of samples annealed at  $T_{\text{Ann}}$  higher than 450 °C show a marked irreversibility. For instance,  $\mu_0 H_C \sim 50$  mT for ZFO-620 (Fig. 4(a)).

Figs. 5 (a) and (b) show the ZFC and FC magnetization curves of some selected samples.  $M_{\text{ZFC}}$  of ZFO shows a rather sharp cusp at  $T_{\text{max}} \sim 14$  K (Fig. 5 (a)), while  $dM_{\text{ZFC}}/dT$  has a

maximum at  $\sim 11$  K (Fig. 5 (c)), i. e., nearby  $T_N$  of normal  $\text{ZnFe}_2\text{O}_4$ . Further,  $M_{\text{ZFC}}$  also shows a convex line comprising the 45-150 K range that is also visualized in its derivative shown in Fig. 5 (c). For ZFO-250 the cusp of  $M_{\text{ZFC}}$  occurs at almost the same  $T_{\text{max}} \sim 14$  K, while samples annealed at higher  $T_{\text{Ann}}$  present a more rounded peak at  $T_{\text{max}}$  (Fig. 5 (a)). In all cases,  $dM_{\text{ZFC}}/dT$  has a peak at about 11 K (Figs. 5 (c) and (d)), with an additional contribution centered at about 22 K for ZFO-580 and ZFO-620 (Figs. 5 (d)). The rate of change of  $M_{\text{ZFC}}$  also shows additional local extremes at higher temperatures (see insets Fig. 5 (c) and (d)). On the other hand, the cusp of  $M_{\text{FC}}$  lies in the 12-14 K range. In all cases,  $M_{\text{FC}}$  decreases monotonically when lowering the temperature below the cusp, a behavior that is usually observed in spin-glass or cluster-glass compounds [29]. A non null difference  $\Delta M = M_{\text{FC}} - M_{\text{ZFC}}$  exists below the irreversibility temperature  $T_{\text{irr}}$ , which is  $T_{\text{irr}} = 120$  K and 230 K, for ZFO and ZFO-370, respectively. In the case of ZFO-620, the irreversibility is observed from ambient temperature.

Figure 6 (a) shows the in-phase  $\chi'$  component of the AC-susceptibility measured at a frequency of 835 Hz. The temperature at which the  $\chi'$  maximum occurs ( $T_m^\chi$ ) allows identifying a magnetic feature of the system such as the magnetic ordering temperature of a compound, the blocking temperature ( $T_B$ ) of particle moments in magnetic nanoparticles, or the freezing temperature ( $T_f$ ) in spin glasses. In our case,  $\chi'$  shows, depending on  $T_{\text{Ann}}$ , one or two distinguishable broad peaks (Figs. 6 (a) and (b)). Indeed, two peaks can be observed for  $\chi'$  of ZFO and for those samples treated up to  $T_{\text{Ann}} = 250$  °C. At higher  $T_{\text{Ann}}$  only one broad peak was considered, except for ZFO-490 and ZFO-540 that also have two resolved peaks (Fig. 6 (b)). On the other hand, the  $\chi'$  magnitude progressively decreases for samples

annealed up to  $T_{Ann}= 370$  °C, while for samples above this  $T_{Ann}$  increases. Furthermore,  $\chi'$  of ZFO-620 far exceeds the response registered for ZFO-370 (Fig. 6(a)). In all cases, the inverse of the susceptibility (not shown) deviates from a Curie-Weiss behaviour below  $\sim 250$ - $280$  K. For instance, the  $\Theta_{CW}$  estimated for ZFO, ZFO-370 and ZFO-620 are about  $+230$ ,  $+80$  and  $+180$  K, respectively.

In all cases,  $T_m^\chi$  shifts to higher temperatures and  $\chi'(T_m^\chi)$  decreases with the frequency (see, for instance, Fig. 6 (b)). The linear fit performed on the Néel-Arrhenius plots for the multi-frequency AC-susceptibility (not shown) gave unphysical values for the attempting time  $\tau_0$ , i. e., by assuming a relaxation time  $\tau = \tau_0 \cdot \exp(E_A/k_B T)$  where  $E_A$  is the barrier energy and  $k_B$  is the Boltzmann constant.

Figure 7(a) shows a representative temperature ( $T_{ex}$ ) of the susceptibility obtained by extrapolating the linear behaviour of  $T_m^\chi$  vs.  $f$  to an exciting field frequency of 1 Hz. We observe that for ZFO (with two resolved contributions),  $T_{ex1}=60$  K and  $T_{ex2}=90$  K. Samples annealed at  $T_{Ann}$  higher than  $250$ °C have low  $\chi'$  values while their unique  $T_{ex}$  remains in the  $45$  to  $60$  K range (Fig.7(a)). For  $T_{Ann}$  above  $450$  °C there is a progressive increment of both  $\chi'$  and  $T_{ex}$ , and the latter tends to a temperature of about  $90$  K.

The relative shift  $\Delta T_{max}/T_{max}$  per decade of frequency quantified throughout the  $p$  parameter allows to roughly identifying the origin of a dynamic magnetic response, i. e., whether is associated to S-G spin-glass ( $0.005 < p < 0.02$ ), C-G cluster-glass ( $0.03 < p < 0.06$ ) or superparamagnetic SPM behaviors ( $p > 0.08$ ) [29]. In our case, the pair of  $p$  values (associated with  $T_{ex1}$  nearby  $60$  K and  $T_{ex2}$  nearby  $90$  K) of samples treated up to  $240$  °C lie at the bottom of C-G region ( $T_{ex1}$ ) and at the S-G region ( $T_{ex2}$ ). The  $p$  values for ferrites

annealed from about 250 to 430 °C –with only one resolved maximum- mainly lie inside the C-G region (Fig. 7(b)). For samples annealed above 490 °C, the  $p$  parameters also correspond to the C-G zone.

#### 4. Discussion

The results from the various characterization techniques confirm that the starting sample ZFO is slightly inverted. Amongst the magnetic features that present this sample are the cusp of  $M$ - $T$  curves at a temperature near the  $T_N$  of the normal Zn-ferrite, two resolved  $\chi'$  maxima, a convex shape of  $M_{FC}$  and  $M_{ZFC}$  at around 50 K, the deviation from the Curie-Weiss law and a positive and high  $\Theta_{CW}$  (+230 K). Considering the XMCD results we infer that the cation inversion involves -at least- the grain surface regions. A weak ferromagnetic response at room temperature is commonly detected in nominal normal bulk  $ZnFe_2O_4$  (see for instance, Refs. [3,30]). This is attributed to a low inversion at surface regions with interrupted super-exchange paths that release the frustration of  $Fe^{3+}$  spins at B sites [3].

The slight frequency dependency of the  $\chi'$  maximum of ZFO (and also for those samples treated under vacuum up to about 250 °C) accounts for a glassy behavior. A disorder state in Zn-ferrite can be associated to: i) an intrinsic defect-free behavior due to regions with short-range spin correlations promoted by FM  $J_1$  interactions, which compete with AF  $J_3$  interactions [4,6], and ii) the slight degree of inversion of these samples which gives rise to modified first nearest-neighbor  $J_1'$  AF interactions that compete with also modified third-neighbor  $J_3'$  ones both now involving  $Fe^{3+}$  at (A) and [B] sites [5, 30]. On the other hand,  $\chi'$  measurements down to 2 K (see S. I. and Fig. 8) reflect the  $J_3$  predominance below 15 K because  $\chi'$  becomes independent on the frequency of the exciting magnetic field.

Vacuum annealing above 250 °C causes that the iron ions start leaving the initial non-equilibrium (A) sites to occupy the [B] ones and, at the same time,  $\text{Zn}^{+2}$  ions only occupy their preferential (A) positions. At  $T_{\text{Ann}}$  above *ca.* 325°C the detection of inversion is negligible. Thus, the cation distribution approaches to that expected for a normal ferrite state and, consequently, there is a detriment of its magnetic response. In addition, the two  $\chi'$  maxima  $T_{ex1}$  (~60 K) and  $T_{ex2}$  (~90 K) merge into one resolved broad maximum that lies in the 45 to 60 K range. Likewise  $T_{ex1}$ , the frequency-shift of this unique  $\chi'$  maximum implies that  $p$  lies in the C-G region, accounting for a disordered magnetic behavior of defective  $\text{ZnFe}_2\text{O}_{4-\delta}$ , where  $\delta$  denotes the presence of VO generated by the annealing under vacuum.

Considering the allocation of cations and their magnetic responses, ZFO-370 and ZFO-408 would approach more than the other samples to a normal Zn-ferrite. Then, it is worthwhile describing their magnetic behavior more in detail. Figure 8 (a) shows the AC susceptibility measured in the 2 to 120 K range for ZFO-370. The distinction of temperature ranges displayed in Fig. 8 highlights the predominance of each type of interaction. This is schematized using the spin dodecamer model that is formed on the (111) kagome plane [8]. Below 15 K we observe that  $\chi'$  does not depend on the frequency and shows a cusp at ~ 13 K. The ZFC and FC curves (Fig. 8 (b)) deviate from each other and both drop with decreasing the temperature. Such behaviors resemble those found in spin glasses [10,29] and, for this geometrically frustrated compound they are probably related to the prevalence of interaction  $J_3$  over  $J_1$  without attaining a long-range ordering [9]. At intermediate temperatures (from 15 to 85 K)  $\chi'$  has a broad peak centered at about 45 K that slightly varies with the frequency, while  $M_{\text{ZFC}}$  and  $M_{\text{FC}}$  differ noticeably. The relative shift of this peak quantified through the  $p$  parameter is compatible with a C-G behaviour in a

temperature range where the spin interactions are governed by  $J_1$  [9]. Finally, at temperatures higher than 85 K, the thermal energy is high enough to overcome the spin interactions and a typical Curie-Weiss behavior is observed (Fig. 8). The progressive extinction of the  $\chi'$  broad peak at  $T_{ex2}$  when  $250 < T_{Ann} < 450$  °C coincides with the recovery of cation equilibrium positions at the grain surface, as shown by XMCD. Thus, it is plausible that  $T_{ex2}$  is related to the freezing of spins at regions with a partial inversion, more visible in sample ZFO.

Ferrites treated at  $T_{Ann} \sim 450$  °C and above display a ferromagnetic response (Fig. 4). The main magnetic characteristics are the S-shaped  $M$  vs.  $H$  loops with a  $M_s$  that increases with  $T_{Ann}$ , the irreversibility at room temperature, the shift to higher temperatures of the maximum of  $M_{ZFC}$  with  $T_{Ann}$ , a broad  $\chi'$  maximum,  $p$  parameters lying in the S-G or C-G region and positive and high  $\Theta_{CW}$ . Therefore, vacuum annealing at these  $T_{Ann}$  causes a cation redistribution with both Zn and Fe at non-equilibrium sites. But the more remarkable effect is the large increment of  $Fe^{3+}$  at B sites shown by the XMCD results. In the present case, it is expected that the thermal annealing under vacuum above a certain  $T_{Ann}$  produces VO. Indeed, the progressive darkening of the samples with  $T_{Ann}$  (see S. I.) as well as the trend showed by the Mössbauer hyperfine parameters [31] can be interpreted in terms of the formation of VO. To maintain the charge neutrality, the excess of negative charge in  $ZnFe_2O_{4-\delta}$  could be compensated by a reduction of iron ions from  $Fe^{3+}$  to  $Fe^{2+}$  or due deficiency of Zn, the latter giving rise to a non-stoichiometric compound. However, these two possibilities were below the detection limit of our experiments.

All in all, these vacancies add randomness related with its position and frustration due to the competitive interactions modified by broken paths that give rise to a FM coupling

between  $\text{Fe}^{3+}$  at B sites through  $J_1''$  (B-VO-B) [14] as well as  $J_3''$  (B-VO-B-O-B or B-VO-A-O-B). The partial recovery of the inversion at these  $T_{\text{Ann}}$  can be related to a way of releasing the strain caused by a higher concentration of VO [12,17,32].

## 5. Conclusions

$\text{ZnFe}_2\text{O}_4$  prepared by solid-state reaction (ZFO) showed a magnetic behavior linked to its low inversion state depicted by a weak ferromagnetic response and a thermal dependency of the magnetization with a cusp at 13 K. The AC-susceptibility has two maxima at ~60 K and ~90 K, whose frequency variation is indicative of a glassy behavior associated to the intrinsic and extrinsic frustration due to competing interactions.

Upon thermal treatment performed under vacuum the electronic and magnetic behavior change in accordance to the production of defects such as oxygen vacancies and redistribution of cations. For  $T_{\text{Ann}}$  higher than 250 °C the  $\text{Fe}^{3+}$  and  $\text{Zn}^{2+}$  ions at the grain surface start leaving their non-equilibrium sites and the ferrite magnetic state approaches to a normal configuration. The magnetic response decreases when  $250 < T_{\text{Ann}} < 450$  °C, the unique resolved  $\chi'$  maximum lies within the 45 to 60 K range and its frequency-shift is consistent with a cluster-glass behaviour. In particular, the magnetic behaviour of these ferrites with allocation of cations  $\text{Fe}^{3+}$  and  $\text{Zn}^{2+}$  only at their equilibrium sites allows identifying the prevalence of each super-exchange interactions that operate in this geometrically frustrated  $\text{ZnFe}_2\text{O}_4$  compound. Finally, annealing at  $T_{\text{Ann}}$  higher than 450 °C generates an oxygen deficiency accompanied by a slight recovery of the inversion. A remarkable result on these samples is the increment of  $\text{Fe}^{3+}$  magnetic coupling at octahedral sites and the enhanced magnetic response of these defective zinc ferrites.



**Acknowledgements:** This work was supported by CONICET and ANPCyT (PICT 2616 and PICT 2618), Argentina

## References

- [1] J. Smit and H.P.J. Wijn, Ferrites, Philips Technical Library, Eindhoven, The Netherlands, 1959.
- [2] W. Schiessl, W. Potzel, H. Karzel, M. Steiner, G. M. Kalvius, A. Martin, M. K. Krause, I. Halevy, J. Gal, W. Schäfer, G. Will, M. Hillberg, and R. Wäppling, Magnetic properties of the  $\text{ZnFe}_2\text{O}_4$  spinel. *Phys. Rev. B* 53 (1996) 9143-9152.
- [3] T. Usa, K. Kamazawa, H. Sekiya, S. Nakamura, Y. Tsunoda, K. Kohn, K., & M. Tanaka, Magnetic properties of  $\text{ZnFe}_2\text{O}_4$  as a 3-D geometrical spin frustration system, *J. Phys. Soc. Japan* 73 (2004) 2834-2840.
- [4] K. Kamazawa, Y. Tsunoda, H. Kadowaki and K. Kohn, Magnetic neutron scattering measurements on a single crystal of frustrated  $\text{ZnFe}_2\text{O}_4$ , *Phys. Rev. B* 68 (2003) 024412
- [5] M. A. Hakim, M. M. Haque, M. Huq and P. Nordblad, Spin-glass-like ordering in the spinel  $\text{ZnFe}_2\text{O}_4$  ferrite, *Physica B: Cond. Matt.* 406 (2011) 48-51.
- [6] T. Watanabe, S. Tadataka, K. Tomiyasu, K. Kamazawa, Acoustic study of dynamical molecular-spin state without magnetic phase transition in spin-frustrated  $\text{ZnFe}_2\text{O}_4$ , *Phys. Rev. B* 92, (2015) 174420.
- [7] S-H. Lee et al., Frustrated magnetism and cooperative phase transitions in spinels, *J. Phys. Soc. Japan* 79 (2010) 011004
- [8] K. Tomiyasu and K. Kamazawa, A Spin Molecule Model for Geometrically Frustrated Spinel  $\text{ZnFe}_2\text{O}_4$ , *J. Phys. Soc. Jpn.* 80 (2011), SB024
- [9] Y. Yamada, K. Kamazawa and Y. Tsunoda, Interspin interactions in  $\text{ZnFe}_2\text{O}_4$ , Theoretical analysis of neutron scattering study. *Phys. Rev. B* 66 (2002), 064401-
- [10] H. Mamiya, N. Tsujii, N. Terada, S. Nimori, H. Kitazawa, A Hoshikawa, and T. Ishigaki, Slow dynamics in the geometrically frustrated magnet  $\text{ZnFe}_2\text{O}_4$ : Universal features of aging phenomena in spin glasses. *Phys. Rev. B* 90 (2014) 014440.
- [11] S. J. Stewart, S. J. A. Figueroa, J. M. Ramallo López, S. G. Marchetti, J. F. Bengoa, R. J. Prado, F. G. Requejo, Cationic exchange in  $\text{ZnFe}_2\text{O}_4$  revealed by experimental and simulated near-edge absorption structure, *Phys. Rev. B* 75 (2007) 073408-073411.

- [12] J. Philip, G. Gnanaprakash, G. Panneerselvam, M. P. Antony, T. Jayakumar, and B. Raj, Effect of thermal annealing under vacuum on the crystal structure, size, and magnetic properties of  $\text{ZnFe}_2\text{O}_4$  nanoparticles, *J. Appl. Phys.* 102 (2007) 054305-6
- [13] S. Nakashima, K. Fujita, A. Nakao, K. Tanaka, Y. Shimotsuma, K. Miura, and K. Hirao, Enhanced magnetization and ferrimagnetic behavior of normal spinel  $\text{ZnFe}_2\text{O}_4$  thin film irradiated with femtosecond laser, *Appl. Phys. A* 94 (2009) 83-88.
- [14] C. E. Rodríguez Torres, G. A. Pasquevich, P. Mendoza Zélis, F. Golmar, S. P. Heluani, S. K. Nayak, W. A. Adeagbo, W. Hergert, M. Hoffmann, A. Ernst, P. Esquinazi, S. J. Stewart, Oxygen vacancy-induced local ferromagnetism as a driving mechanism in enhancing the magnetic response of ferrites. *Phys. Rev. B* 89 (2014) 104411-7
- [15] D. Guo, Ch. Jiang, X. Fan, D. Xue, Thermal annealing effect on structural and magnetic properties of  $\text{ZnFe}_2\text{O}_4$  thin films deposited by magnetron sputtering, *Appl. Surf. Sci.* 307 (2014) 576-578
- [16] Y. F. Chen, D. Spoddig and M. Ziese, Epitaxial thin film  $\text{ZnFe}_2\text{O}_4$ : a semi-transparent magnetic semiconductor with high Curie temperature, *J. Phys. D: Appl. Phys.* 41 (2008), 205004.
- [17] Y. Yamamoto, H. Tanaka, T. Kawai, The Control of Cluster-Glass Transition Temperature in Spinel-Type  $\text{ZnFe}_2\text{O}_{4-\delta}$ , Thin Film, *Japanese J. Appl. Phys.* 40 (2001) L545.
- [18] M. Hofmann, S. J. Campbell, H. Ehrhardt and R. Feyerherm, R, The magnetic behaviour of nanostructured zinc ferrite, *J. Mat. Sci.* 39 (2004) 5057-5065.
- [19] H. C. St. O'Neill, Temperature dependence of the cation distribution in zinc ferrite ( $\text{ZnFe}_2\text{O}_4$ ) from powder XRD structural refinements, *European J. Mineralogy* 4 (1992) 571-580.
- [20] A. Pavese, D. Levy and A. Hoser, Cation distribution in synthetic zinc ferrite ( $\text{Zn}_{0.97}\text{Fe}_{2.02}\text{O}_4$ ) from in situ high-temperature neutron powder diffraction, *Am. Mineralogist*, 85 (2000) 1497-1502.
- [21] F. Braestrup, B. C. Hauback, and K. K. Hansen, Temperature dependence of the cation distribution in  $\text{ZnFe}_2\text{O}_4$  measured with high temperature neutron diffraction. *Journal of Solid State Chemistry*, 181 (2008), 2364-2369.
- [22] J. R. Sai, S. D. Kulkarni, S. S. Bhat, N. G. Sundaram, N. Bhat, S. A. Shivashankar, Controlled inversion and surface disorder in zinc ferrite nanocrystallites and their effects on magnetic properties, *RSC Advances* 5 (2015) 10267-10274.
- [23] S. Ayyappan, S. P. Raja, C. Venkateswaran, J. Philip, and B. Raj, Room temperature ferromagnetism in vacuum annealed  $\text{ZnFe}_2\text{O}_4$  nanoparticles, *Appl. Phys. Lett.* 96 (2010) 143106-3.

- [24] J. Yao, Y. Li, X. Li, and X. Zhu, First-Principles Study of the Geometric and Electronic Structures of Zinc Ferrite with Vacancy defect, *Metallurgical and Material Transactions A*, 47 (2016) 3753-3760.
- [25] L. Lutterotti, Total pattern fitting for the combined size-strain-stress-texture determination in thin film diffraction, *Nuclear Inst. and Methods in Physics Research B* 268 (2010) 334-340.
- [26] S. Nakashima, K. Fujita, K. Tanaka, K. Hirao, T. Yamamoto, and I. Tanaka, First-principles XANES simulations of spinel zinc ferrite with a disordered cation distribution, *Phys. Rev. B* 75 (2007), 174443-8.
- [27] M. Wilke, F. Farges, P. E. Petit, G. E. Brown and F. Martin, Oxidation state and coordination of Fe in minerals: An Fe K-XANES spectroscopic study, *Am. Mineralogist* 86 (2001) 714-730.
- [28] Magnetism, Fundamentals, volume 1, Springer, Eds: Lacheisserie, Gignoux, Etienne, 2005, p. 198.
- [29] J. A. Mydosh, *Spin Glass*, London, Taylor & Francis, 1993.
- [30] C. B. R. Jesus, E. C. Mendonça, L. S. Silva, W. S. D. Folly, C. T. Meneses, and J. G. S. Duque, Weak ferromagnetic component on the bulk  $\text{ZnFe}_2\text{O}_4$  compound. *J. Magn. Magn. Mat.* 350 (2014) 47-49.
- [31] J. M. Quintero, K. L. Salcedo Rodríguez, G. A. Pasquevich, P. M. Mendoza Zélis, S. J. Stewart, C. E. Rodríguez Torres, L. A. Errico, Experimental and ab initio study of the hyperfine parameters of  $\text{ZnFe}_2\text{O}_4$  with defects, *Hyp. Int.* 237 (2016), 1-7.
- [32] J. H. Kim, Y. J. Jang, J. H. Kim, J. W. Jang, S. H. Choi, and J. S. Lee, Defective  $\text{ZnFe}_2\text{O}_4$  nanorods with oxygen vacancy for photoelectrochemical water splitting, *Nanoscale* 7 (2015) 19144-19151.

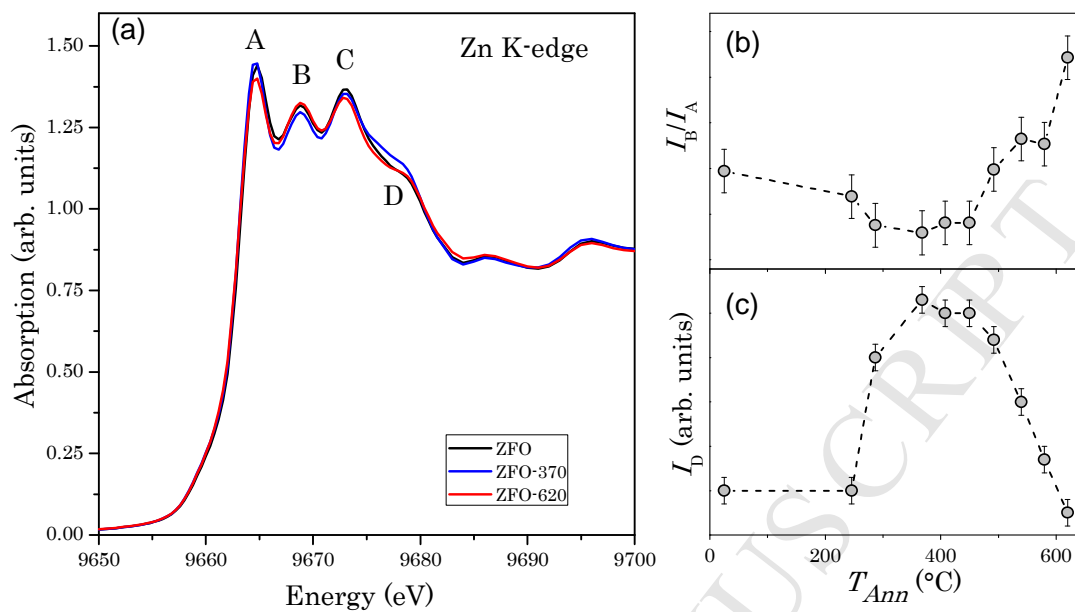


Figure 1: (a) XANES at Zn *K*-edge of samples ZFO, ZFO-370 and ZFO-620, (b) ratio between intensities of peaks B and A ( $I_B/I_A$ ) and (c) intensity of the shoulder D ( $I_D$ ) as a function of the annealing temperature  $T_{Ann}$ .

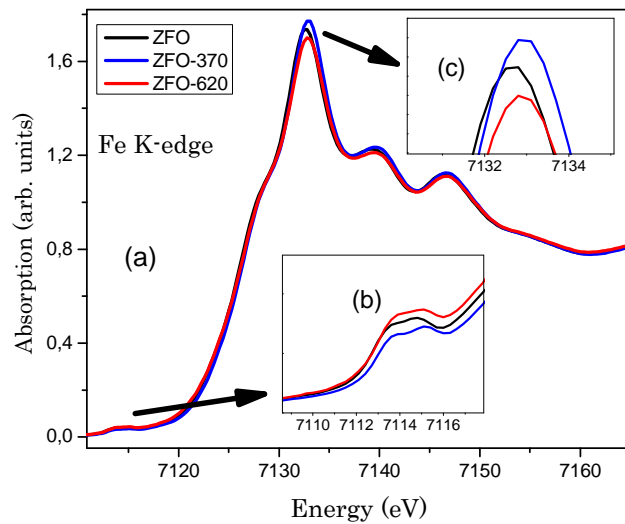


Figure 2: (a) XANES at Fe K-edge of samples ZFO, ZFO-370 and ZFO-620, (b) Enlargement of the pre-peak and (c) white-line regions.

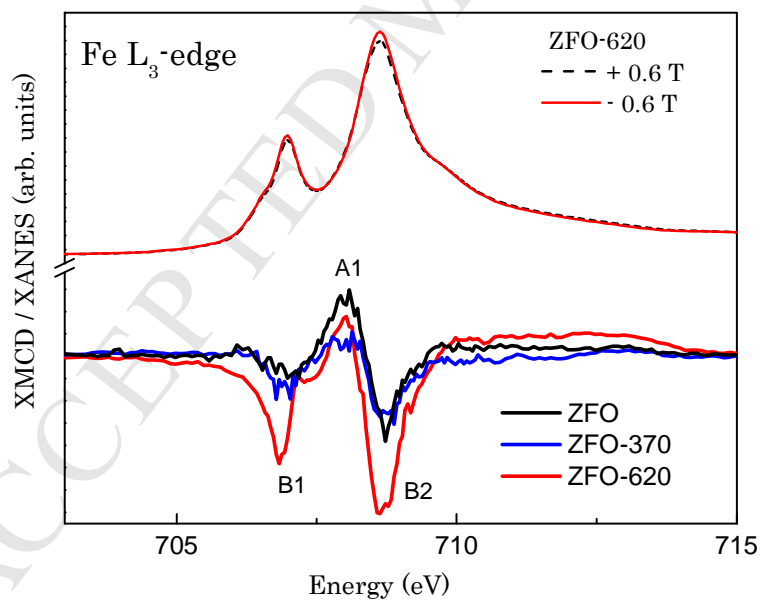


Figure 3: XANES spectra at Fe  $L_3$ -edge for ZFO-620 (under  $\mu_0 H = 0.6$  T) and XMCD signals for samples ZFO, ZFO-370 and ZFO-620.

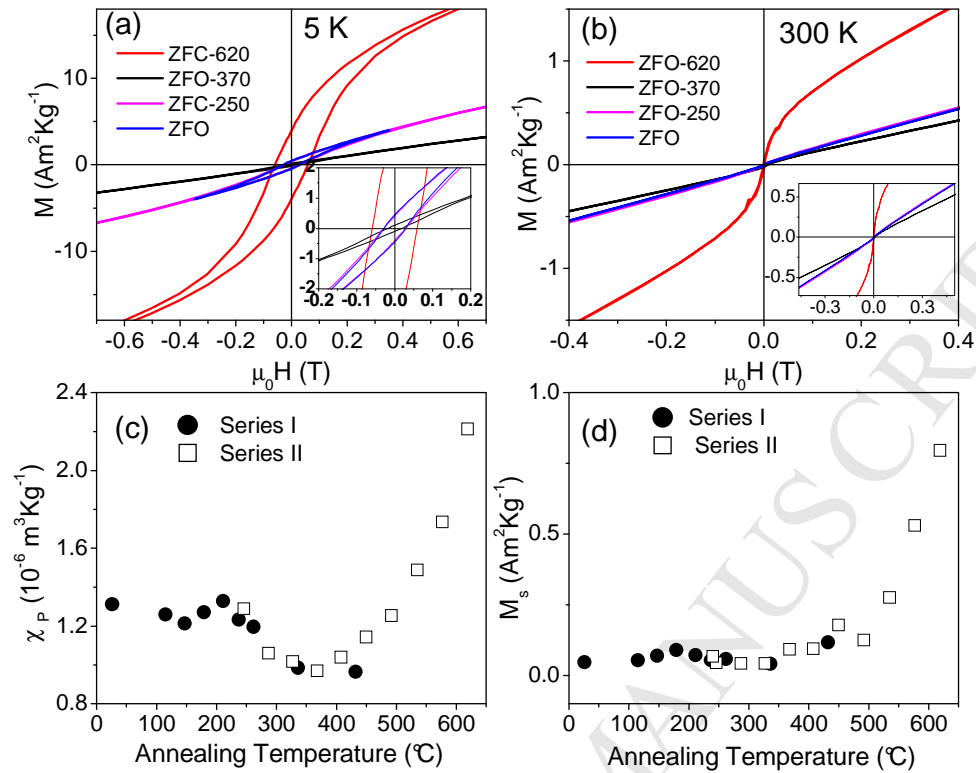


Figure 4:  $M$  vs.  $H$  loops of ZFO, ZFO-250, ZFO-370 and ZFO-620 samples, (a) at 5 K and (b) at 300 K (Inset: An enlargement showing the low-field region), (c) paramagnetic susceptibility  $\chi_P$  and (d) saturation magnetization  $M_s$  for all samples that result from fitting using Eq. (1).

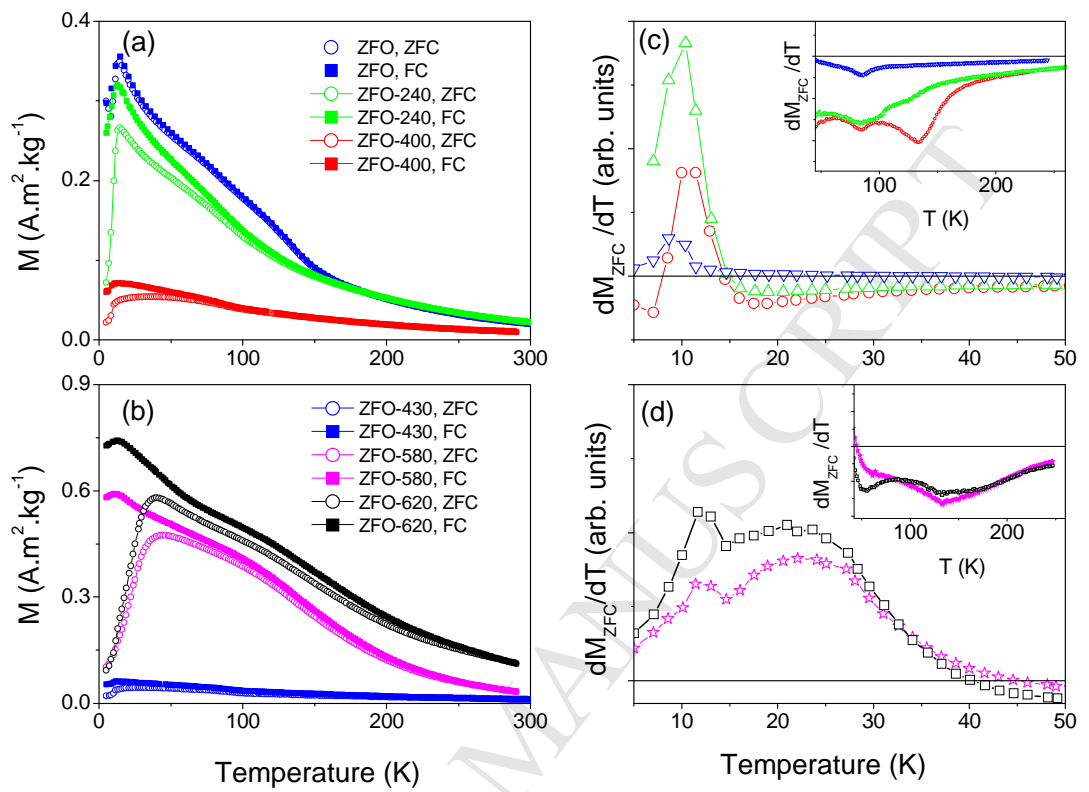


Figure 5: (a) Thermal dependence of the magnetization under ZFC-FC conditions for the samples shown; c), d) rate of change of  $M_{\text{ZFC}}$  corresponding to curves of Figs.(a) and (b), respectively (Insets show a magnification of the 40 to 260 K range).

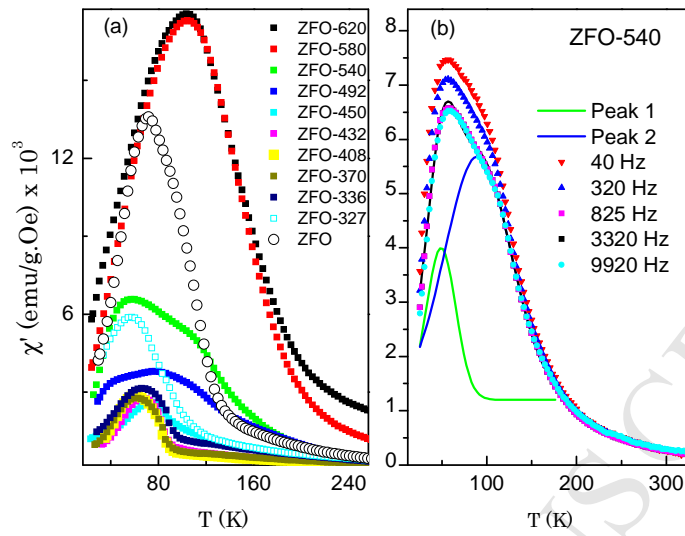


Figure 6: In-phase AC-susceptibility for different ZFO- $T_{\text{Ann}}$  samples measured with a frequency of 825 Hz (a), in-phase susceptibility at different frequencies for sample ZFO-540. Peaks 1 and 2 are the two distinguishable contributions present in this sample used to determine the two  $\chi'$  maxima at  $T_m^\chi$ .



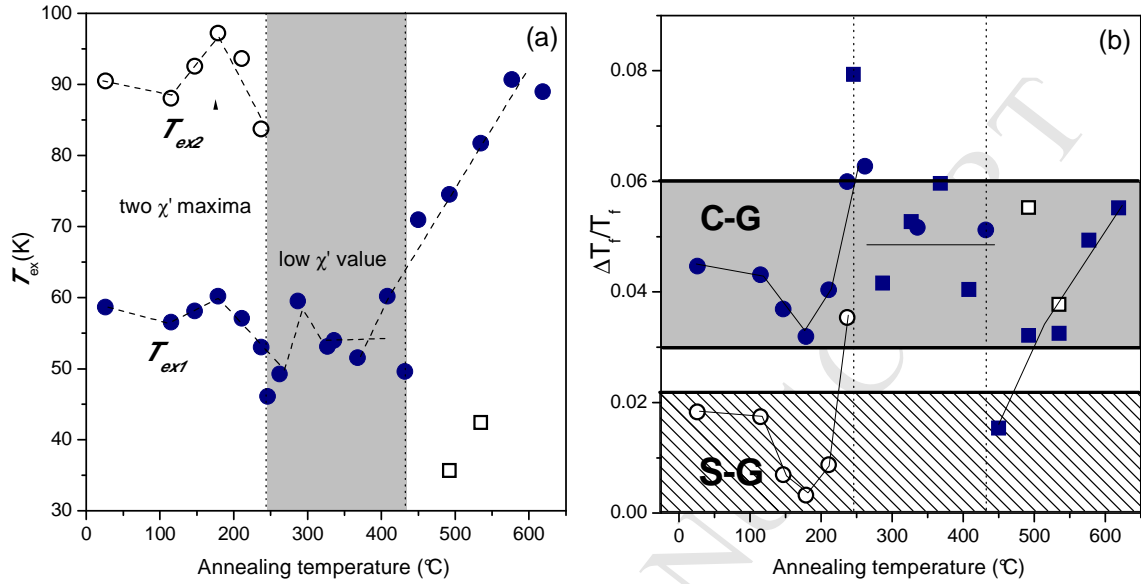


Figure 7: (a) Temperature ( $T_{ex}$ ) that results after extrapolating to  $f=1$  Hz the linear behaviour of  $T_m^\chi$  vs. frequency, (b) Relative shift of temperature ( $\Delta T_m^\chi / T_m^\chi$ ) per decade of frequency ( $p$  parameter), as a function of  $T_{Ann}$ . Cluster-glass C-G and spin-glass S-G reported regions are indicated (Ref.[29]). Circles and square symbols correspond to Series I and II, respectively. For some  $T_{Ann}$ , the hollow and solid symbols account for the two resolved  $\chi'$  maxima at  $T_{ex1}$  and  $T_{ex2}$ .

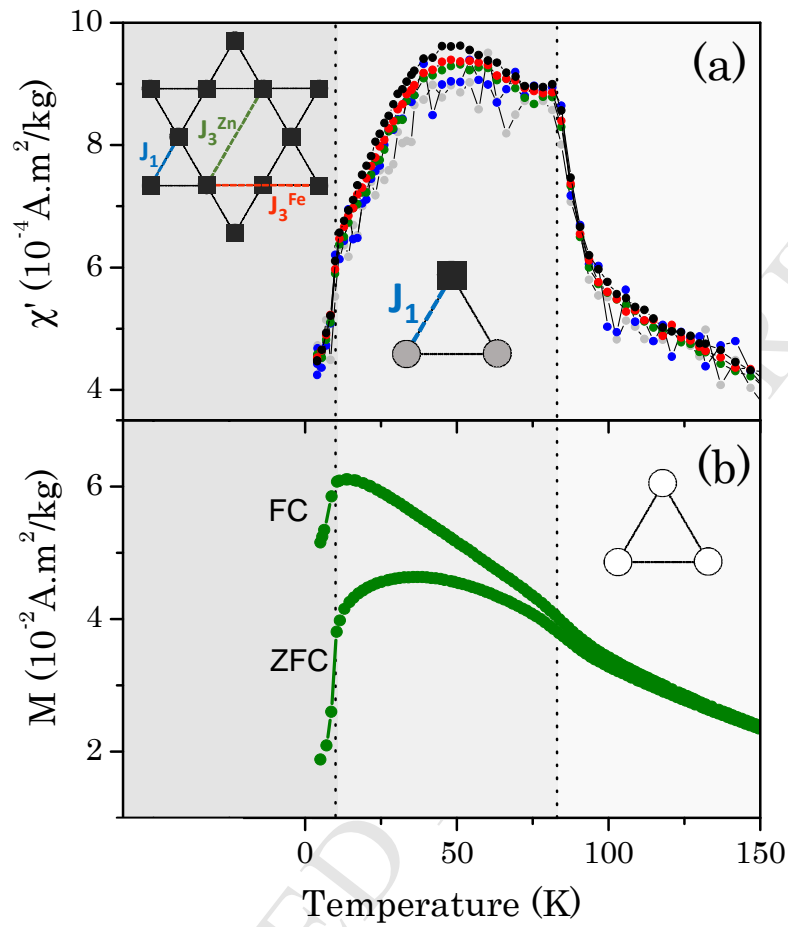
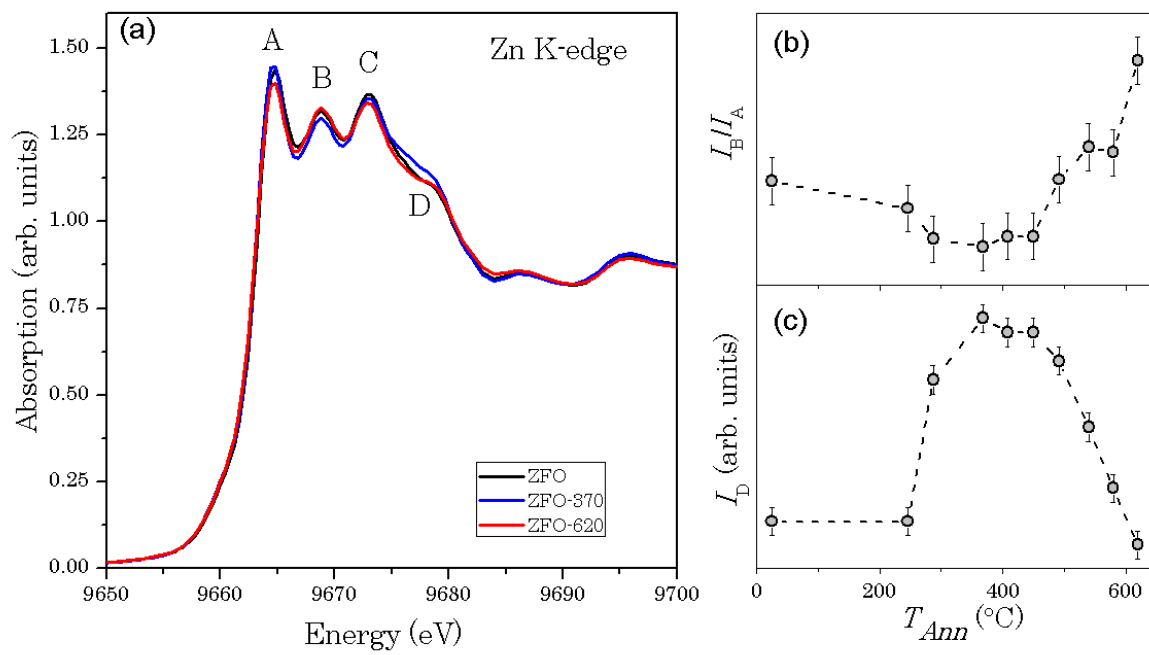
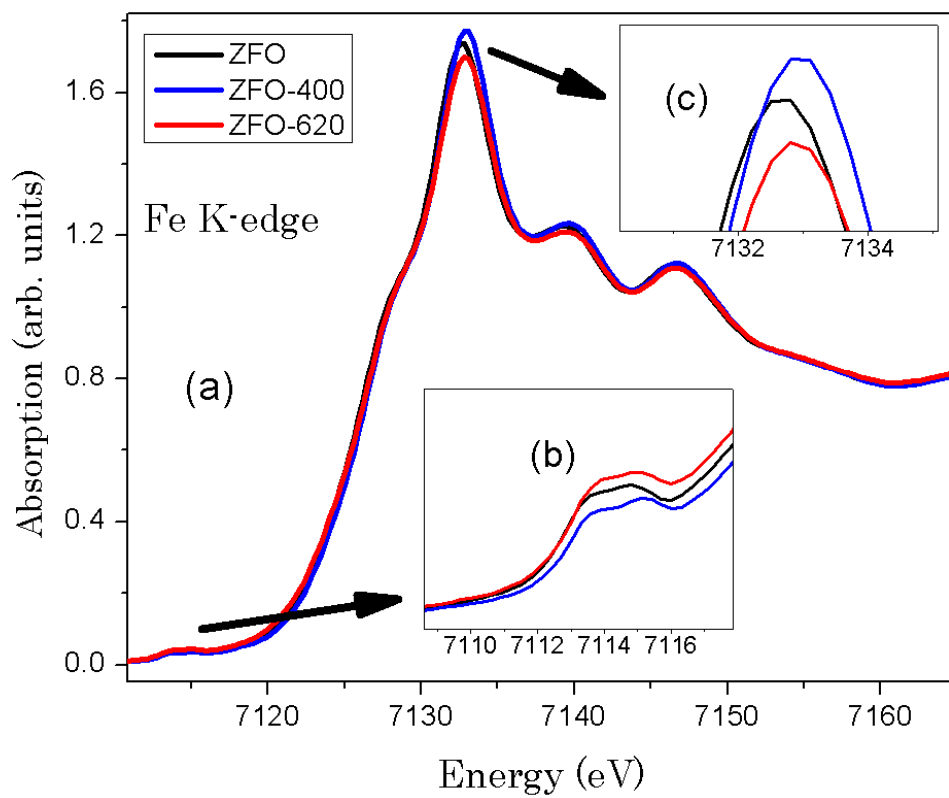
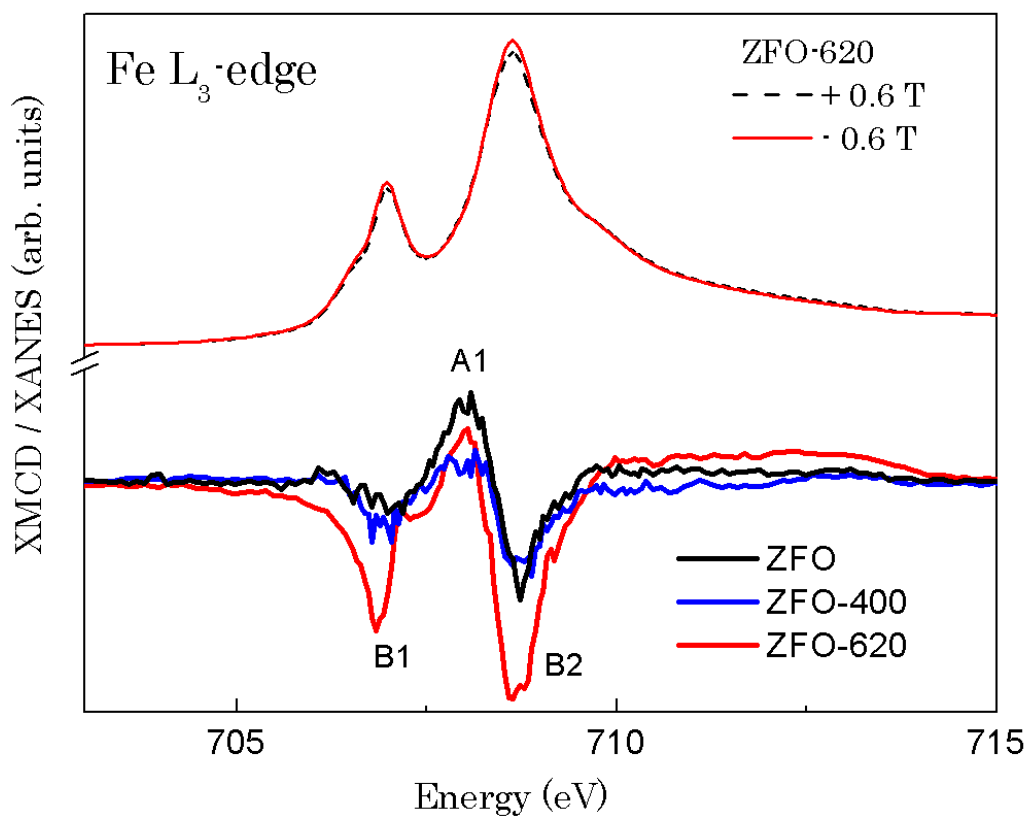
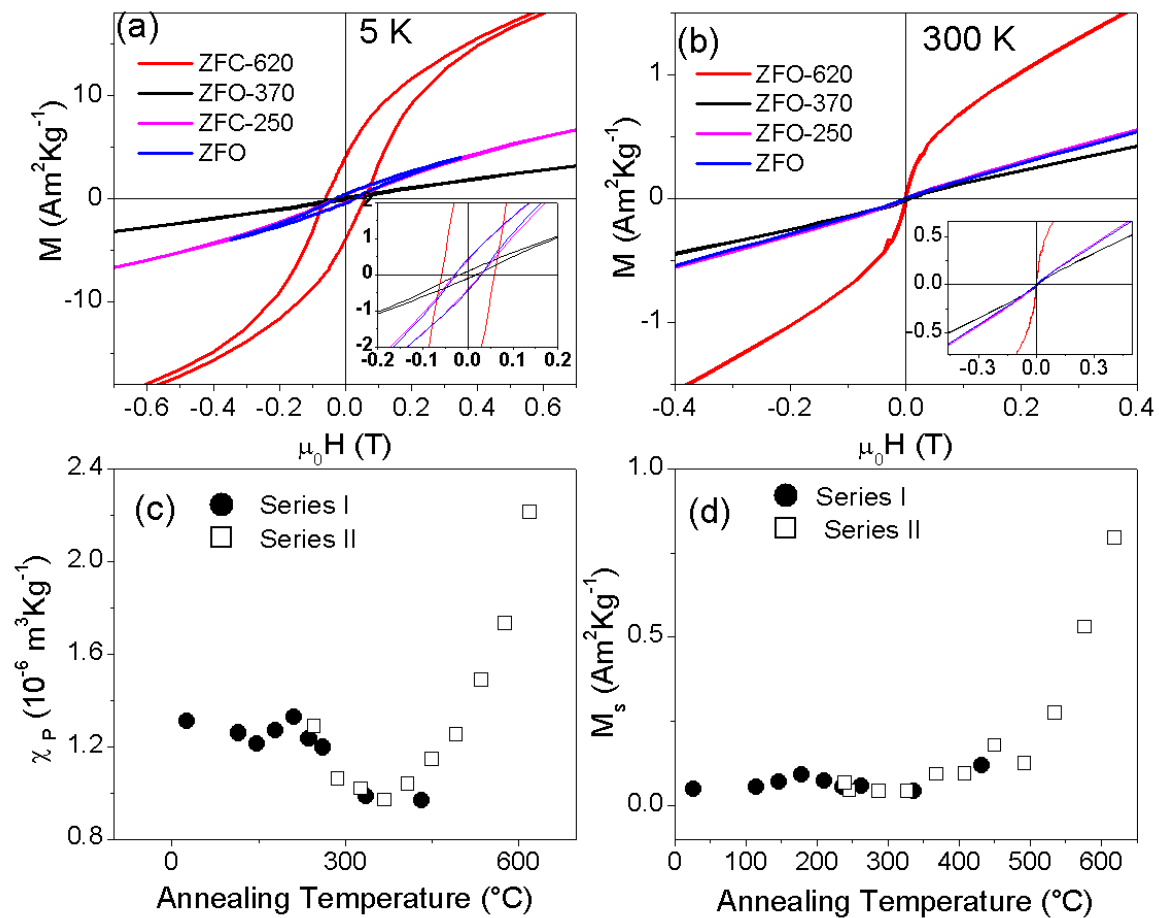


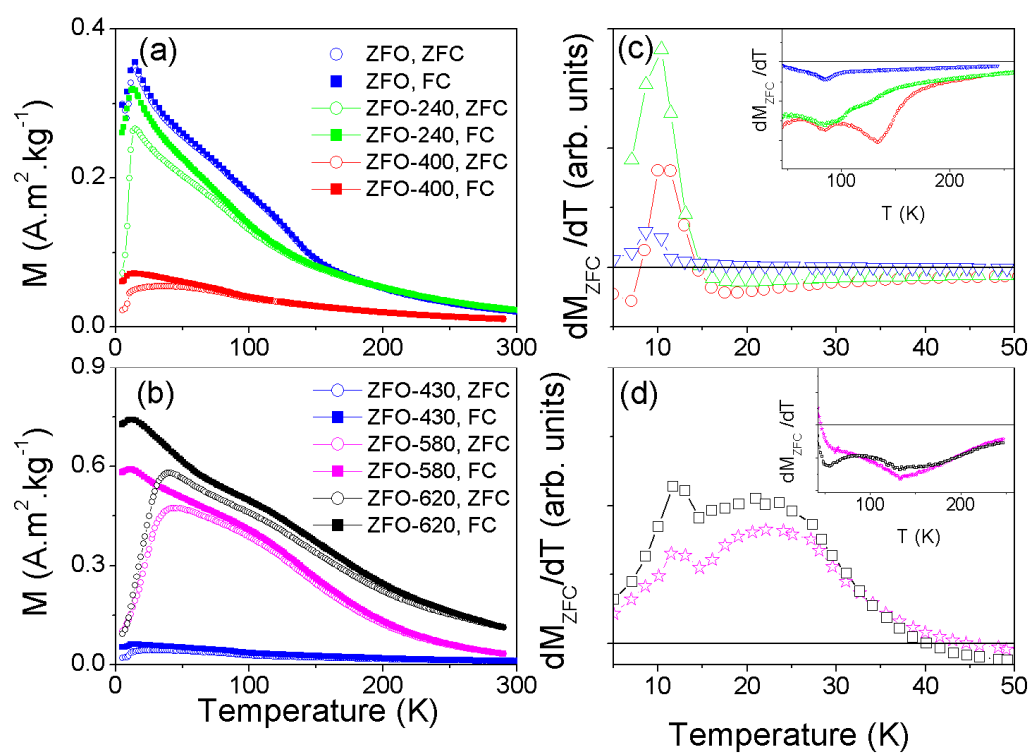
Figure 8: (a) In-phase susceptibility at different frequencies measured between 2 to 150 K for ZFO-370, (b) ZFC-FC magnetization. Dodecamer model showing the  $J_1$  and  $J_3$  interactions (Ref. [8]). Gray dark and light circles represents spin up and down, respectively. White circles at the high temperature region symbolize paramagnetic ions.

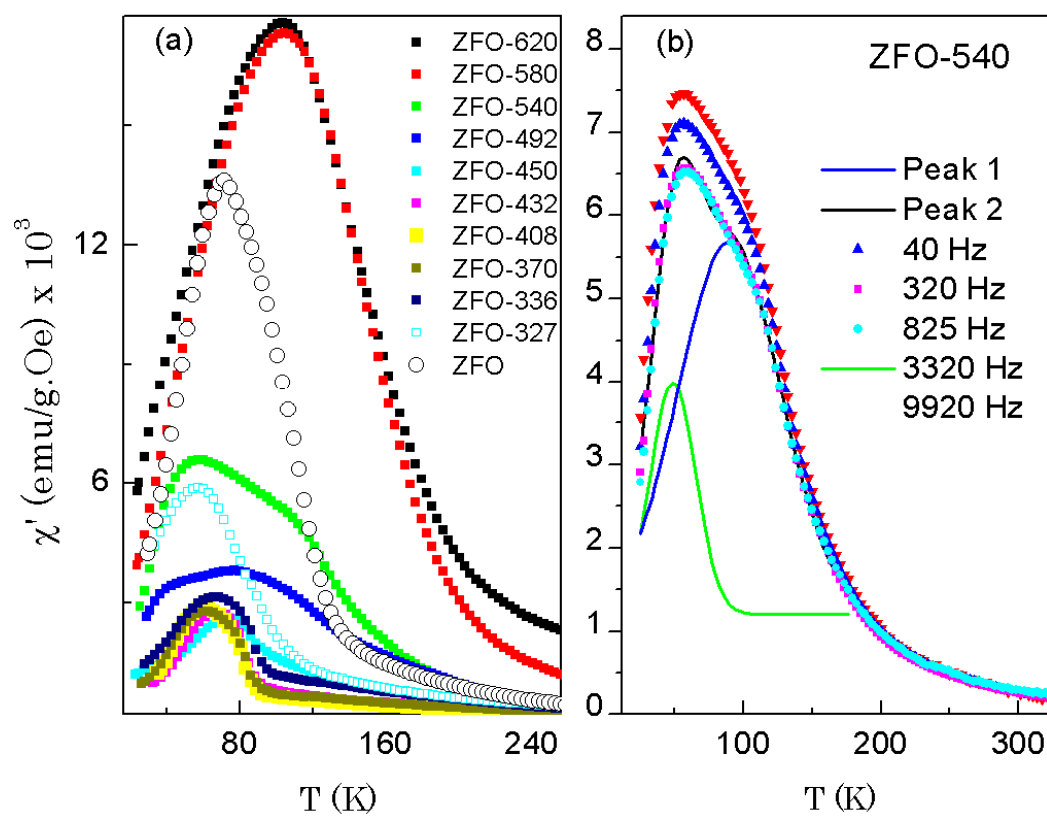






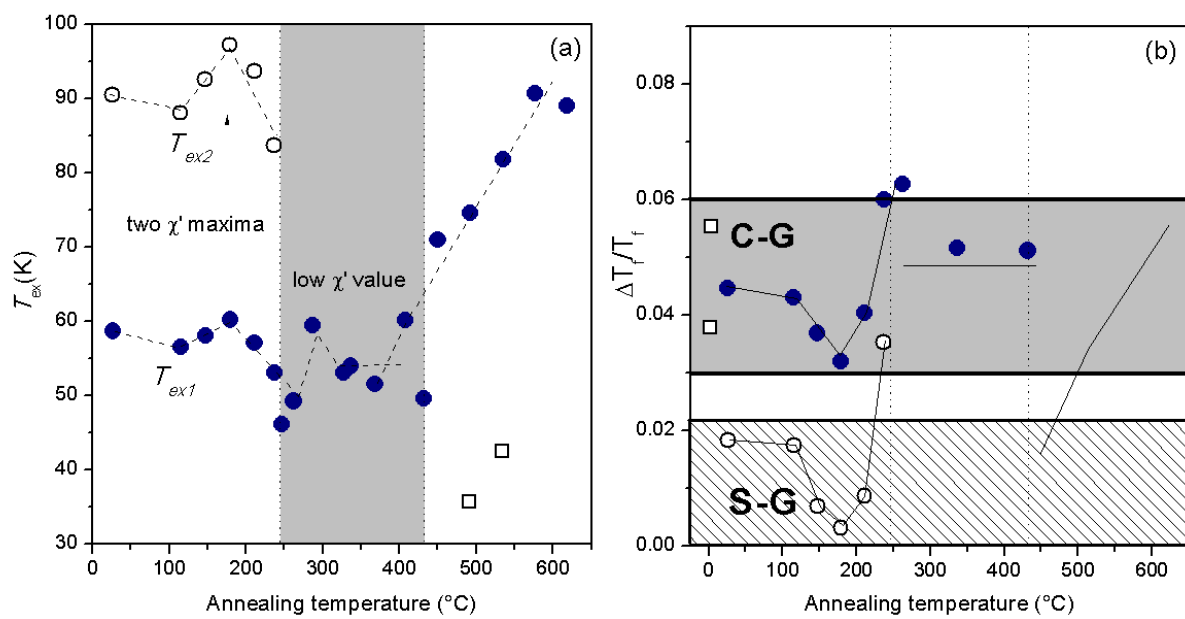


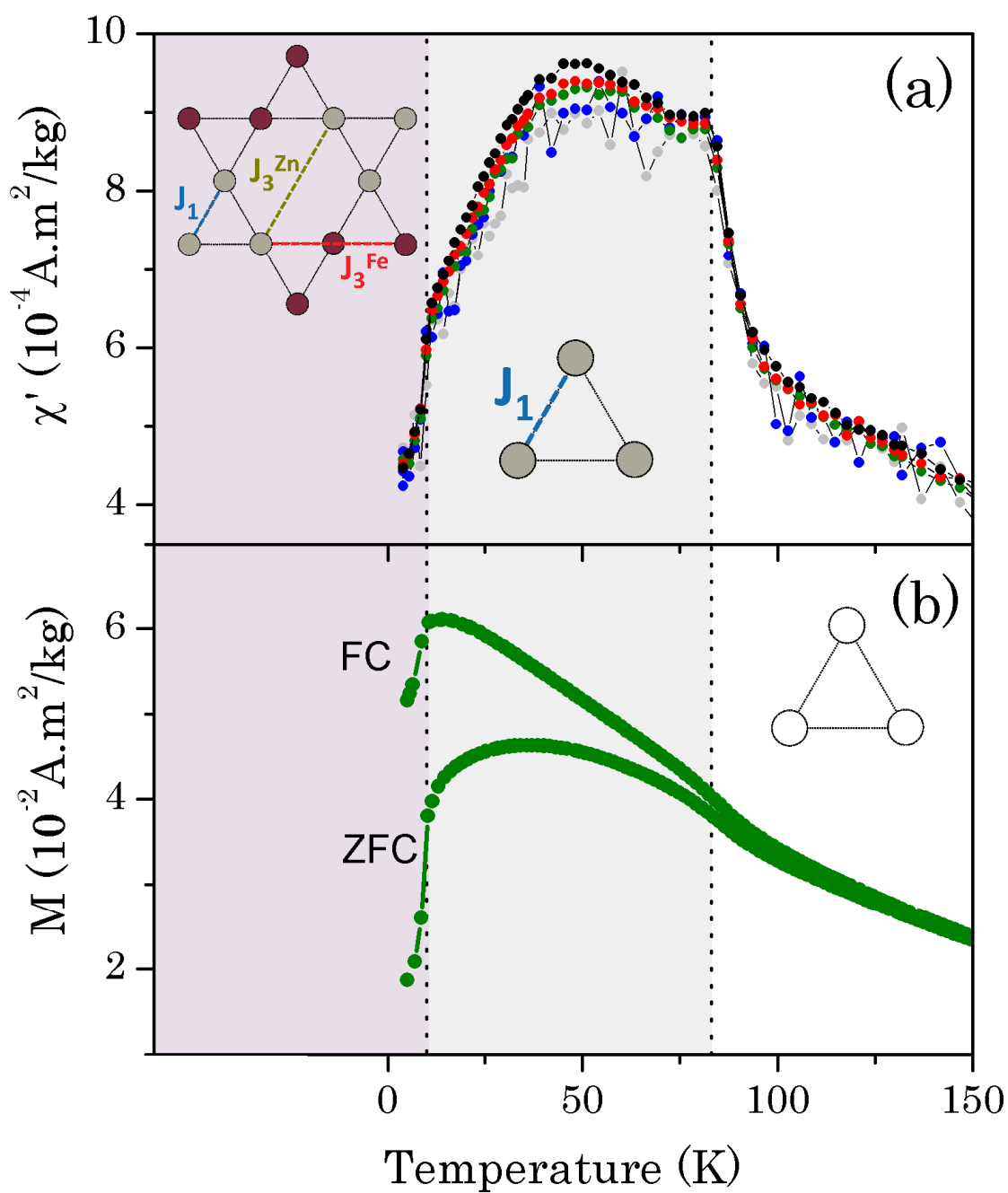




ACCEPTED







**Highlights**

- Defective  $\text{ZnFe}_2\text{O}_{4-\delta}$  samples were obtained by vacuum annealing bulk Zn-ferrite.
- The electronic and magnetic behaviours change with the production of defects.
- The magnetic results accounts for spin-glass and/or cluster-glass behaviour.
- The deficiency of oxygen triggers the coupling between  $\text{Fe}^{3+}$  at octahedral sites.
- AC-susceptibility results allows identifying the prevalence of each interaction.